iScience

CellPress

Article

The FG Loop of PD-1 Serves as a "Hotspot" for Therapeutic Monoclonal Antibodies in Tumor Immune Checkpoint Therapy

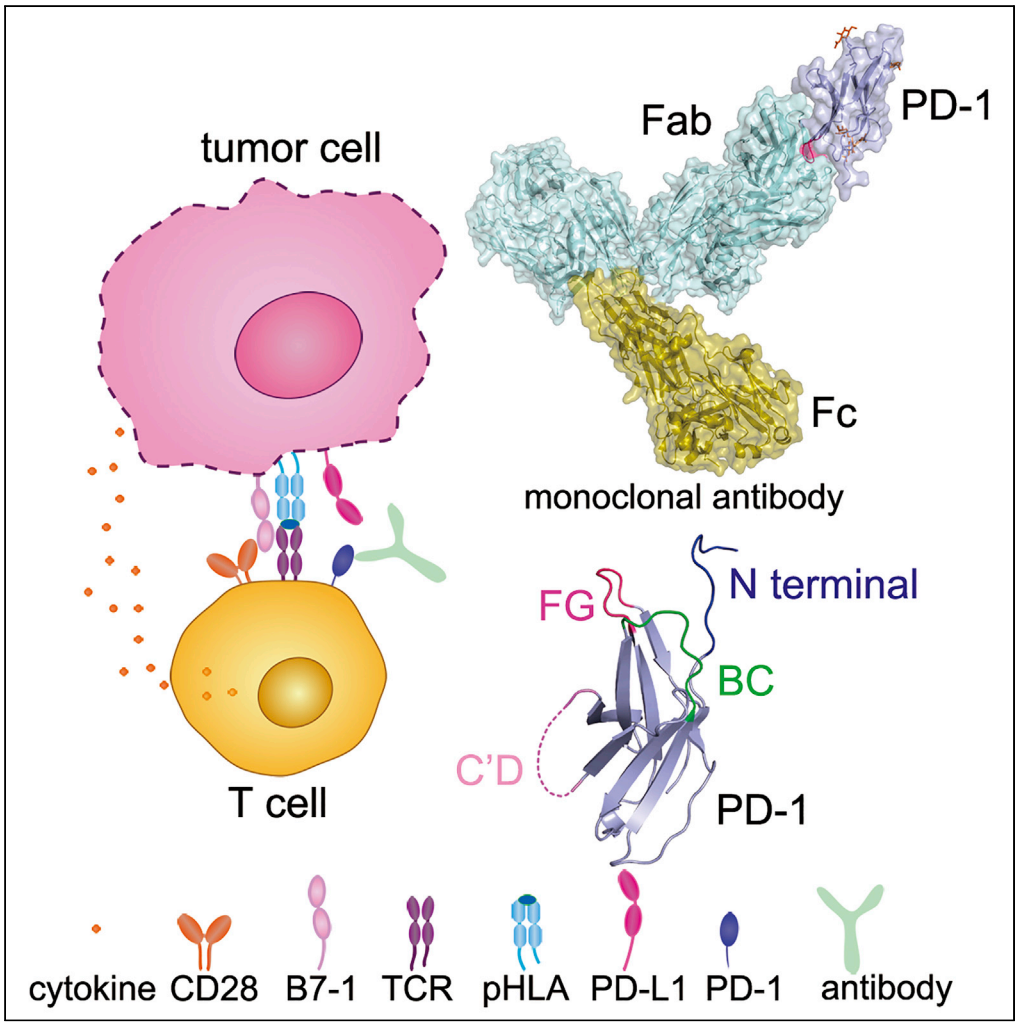

Danqing Chen, Shuguang Tan, Hao Zhang, ..., Minghui Xiao, Jinghua Yan, George F. Gao

yanjh@im.ac.cn (J.Y.)
gaof@im.ac.cn (G.F.G.)

HIGHLIGHTS

GY-5 and GY-14 show efficient anti-tumor efficacy in NCG mouse model

Both GY-5 and GY-14 bind to the FG loop of PD-1

Glycosylation is observed in PD-1, but not involved in binding to GY-5 and GY-14

The loops of PD-1 may serve as "hotspot" for development of PD-1-targeting biologics

DATA AND SOFTWARE AVAILABILITY

6J15
6J14

Chen et al., iScience *14*, 113–124
April 26, 2019
https://doi.org/10.1016/j.isci.2019.03.017

iScience

CellPress

Article

The FG Loop of PD-1 Serves as a "Hotspot" for Therapeutic Monoclonal Antibodies in Tumor Immune Checkpoint Therapy

Danqing Chen,[1,10] Shuguang Tan,[1,10] Hao Zhang,[2,10] Haiyuan Wang,[1,3,10] Weiwu He,[4] Rui Shi,[2] Zhou Tong,[2] Jianhua Zhu,[5] Hao Cheng,[6] Shan Gao,[7] Yan Chai,[1] Jianxun Qi,[1] Minghui Xiao,[8] Jinghua Yan,[1,2,8,9,*] and George F. Gao[1,6,9,11,*]

SUMMARY

Programmed cell death 1 (PD-1)/PD-1 ligand-1 (PD-L1)-blocking monoclonal antibodies (mAbs) have taken center stage for tumor immune checkpoint therapy. Identification of the "hotspots" on PD-1 for mAbs will help to develop next-generation oral deliverable agents with long-lasting efficacy. Here, we identified two PD-1-targeting mAbs, GY-5 and GY-14, with PD-1/PD-L1-blocking efficacy. Complex structural information revealed that both mAbs mainly bind to the FG loop of PD-1, which also contributes multiple interactions with PD-L1. The FG loop adopts substantially varied conformations upon binding to different mAbs, providing a novel targetable region for the development of PD-1-specific biologics and small chemical molecules. Glycosylation modifications of PD-1 could be observed in three of the four potential N-linked glycosylation sites. However, the binding of GY-5 and GY-14 to PD-1 was not affected by glycosylation. These findings broaden our understanding of the mechanism of anti-PD-1 mAbs and provide insight into the development of agents targeting PD-1.

INTRODUCTION

Immune checkpoint therapy (ICT) that targets co-inhibitory or co-stimulatory molecules to modulate anti-tumor T cell reactivity has achieved clinical success since the approval of the cytotoxic T-lymphocyte-associated protein 4 (CTLA-4)-targeting drug ipilimumab by the US Food and Drug Administration (FDA) in 2011 (Callahan et al., 2016; Tan and Gao, 2015). Programmed cell death 1 (PD-1), a member of the CD28-B7 superfamily, is an important co-inhibitory molecule in the modulation of T cell activity (Ishida et al., 1992). PD-1 ligand 1 (PD-L1) and then PD-1 ligand 2 (PD-L2) were subsequently identified as the ligands of PD-1 (Freeman et al., 2000; Latchman et al., 2001; Nishimura et al., 1999). Interruption of the PD-1/PD-L1 interaction with a monoclonal antibody (mAb) to re-stimulate tumor-specific T cell reactivity has been proved to be a promising strategy for treating multiple tumors in clinical applications (Motzer et al., 2015; Robert et al., 2015; Topalian et al., 2012).

The clinical success of anti-PD-1 or anti-PD-L1 mAbs in tumor therapy has initiated an era of anti-tumor drug development to modulate tumor-specific immune responses by targeting immune checkpoint molecules, either co-stimulatory (e.g., 4-1BB) or co-inhibitory (e.g., CTLA-4, PD-1) molecules, to treat tumors (He et al., 2017; Tan and Gao, 2015; Tan et al., 2016). Six mAbs targeting PD-1 or PD-L1 have been approved by the US FDA since 2014 (Tan et al., 2016). However, clinical responsiveness and benefits from these therapies are still limited owing to the disadvantage of the monotherapeutics in highly heterogeneous tumors. Therefore a combination of mAbs targeting varied immune checkpoints or other immune therapeutic strategies, e.g., oncolytic virus and chimeric antigen receptor-engineered T cells, are under evaluation at both the basic research and clinical levels to improve the clinical responsiveness and benefits of the tumor ICT. Looking for mAb replacement like small molecules for convenient drug delivery is another focal point for the field.

The interaction of PD-1 and PD-L1 plays pivotal roles in immune suppression within the tumor microenvironment (Tan and Gao, 2015; Tan et al., 2016). Upregulated PD-L1 expression on tumor cells is correlated with tumor progression and, hence, is a valuable indication for unfavorable prognosis (Iwai et al., 2002; Gridelli et al., 2017). On the other hand, higher PD-L1 levels in tumor tissue indicate better responsiveness

[1]CAS Key Laboratory of Pathogenic Microbiology and Immunology, Institute of Microbiology, Chinese Academy of Sciences, Beijing 100101, China

[2]CAS Key Laboratory of Microbial Physiological and Metabolic Engineering, Institute of Microbiology, Chinese Academy of Sciences, Beijing 100101, China

[3]Laboratory of Animal Infectious Diseases, College of Animal Sciences and Veterinary Medicine, Guangxi University, Nanning 530004, China

[4]OriGene Technologies, Inc., Rockville 20850, USA

[5]Department of Oncology, Fourth Medical Center of PLA General Hospital, Beijing 100048, China

[6]Beijing Institutes of Life Science, Chinese Academy of Sciences, Beijing 100101, China

[7]CAS Key Laboratory of Bio-medical Diagnostics, Suzhou Institute of Biomedical Engineering and Technology, Chinese Academy of Sciences, Suzhou 215163, China

[8]Shanxi Weiqida Guangming Pharmaceutical Co. Ltd., Datong 037301, China

[9]University of Chinese Academy of Sciences, Beijing 100049, China

[10]These authors contributed equally

[11]Lead Contact

*Correspondence: yanjh@im.ac.cn (J.Y.), gaof@im.ac.cn (G.F.G.)

https://doi.org/10.1016/j.isci.2019.03.017

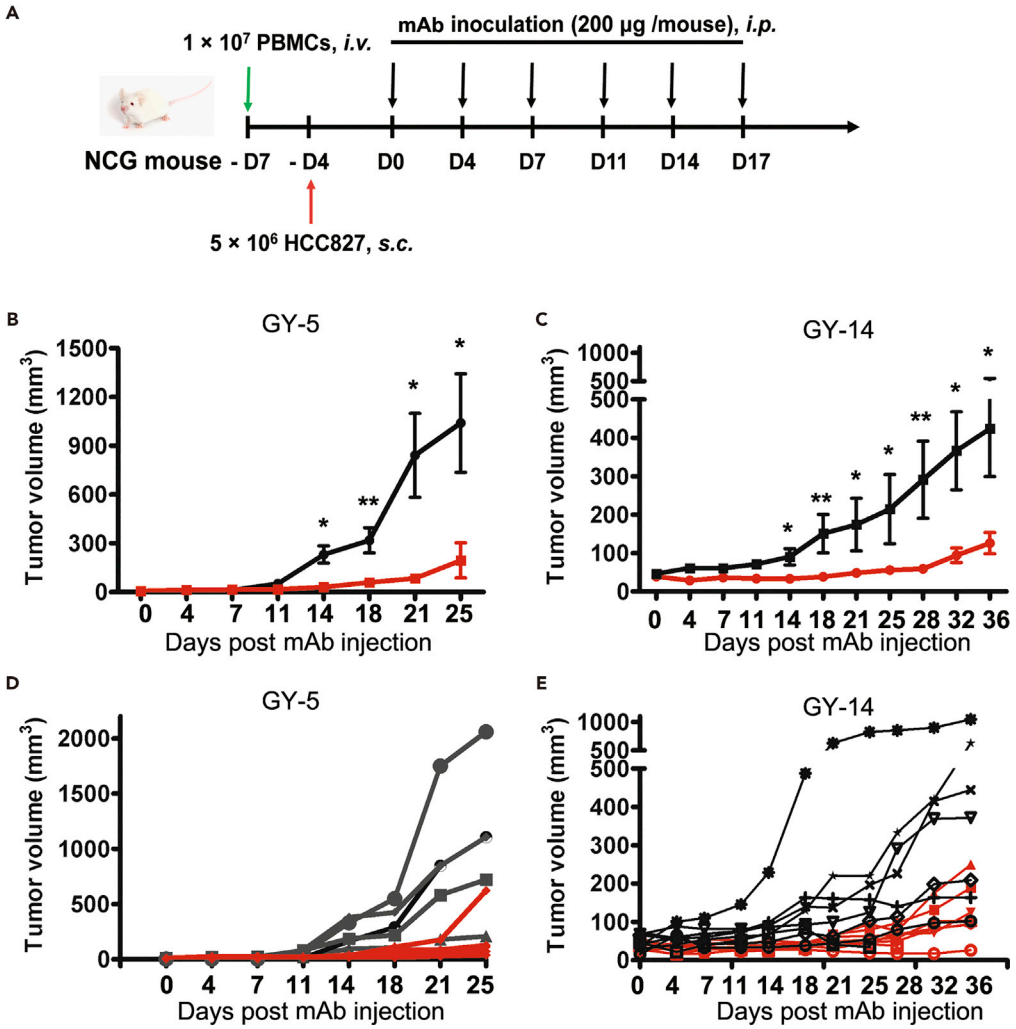

Figure 1. Tumor Suppression Efficacy of the GY-5 and GY-14 mAbs

(A) Flowchart of the animal study. 1×10^7 PBMCs from healthy donors were inoculated intravenously into each NCG mouse, and 5×10^6 HCC-827 cells were inoculated subcutaneously 3 days later. Chimeric GY-5 and GY-14 mAbs were injected intraperitoneally (i.p.) every 3 or 4 days from day 7 (D0) after tumor inoculation. The size of the tumor was monitored every 3 or 4 days after injection of GY-5 or GY-14. An Ebola virus-specific mAb, 13C6, was injected and used as a negative control.

(B and C) Mice bearing subcutaneous HCC-827 tumors for 7 days were treated i.p. with GY-5 at a dose of 200 μg/mouse or control IgG, with five mice for each treatment group (B). Mice bearing HCC-827 tumors for 7 days were treated i.p. with GY-14 at a dose of 200 μg/mouse or control IgG, with eight mice for each treatment group, which was independent of the experiment with GY-5 (C). The data with dot shows the average tumor volume of the group, whereas the SE is presented as longitudinal bars. *$p < 0.05$, **$p < 0.001$. The red line represents the average tumor size of the control IgG treatment group.

(D and E) Tumor sizes of individual mice are presented for GY-5 treatment group (D) and GY-14 treatment group (E) , with each black line showing the changes of the tumor size of a mouse. The red lines represent tumor size of each mouse of control IgG treatment group. The data presented here are representative of two independent experiments with similar results.

See also Figures S1 and S2 and Table S1.

to PD-1/PD-L1 blockade treatment, to a certain extent, in ovarian, kidney, pancreatic, and gastric cancers (Powles et al., 2017; Massard et al., 2016; Apolo et al., 2017; Balar et al., 2016). Inducible PD-1 expression on T lymphocytes (tumor-infiltrating lymphocytes in particular) can lead to the tolerance of tumor-specific T cells to tumors (Tumeh et al., 2014). Moreover, PD-1 has also been found to be expressed in tumor cells, and tumor-cell-intrinsic PD-1 can promote tumorigenesis by modulating downstream mammalian target of rapamycin signaling (Kleffel et al., 2015). Forced expression of PD-1 or PD-L1 on T cells or tumor cells

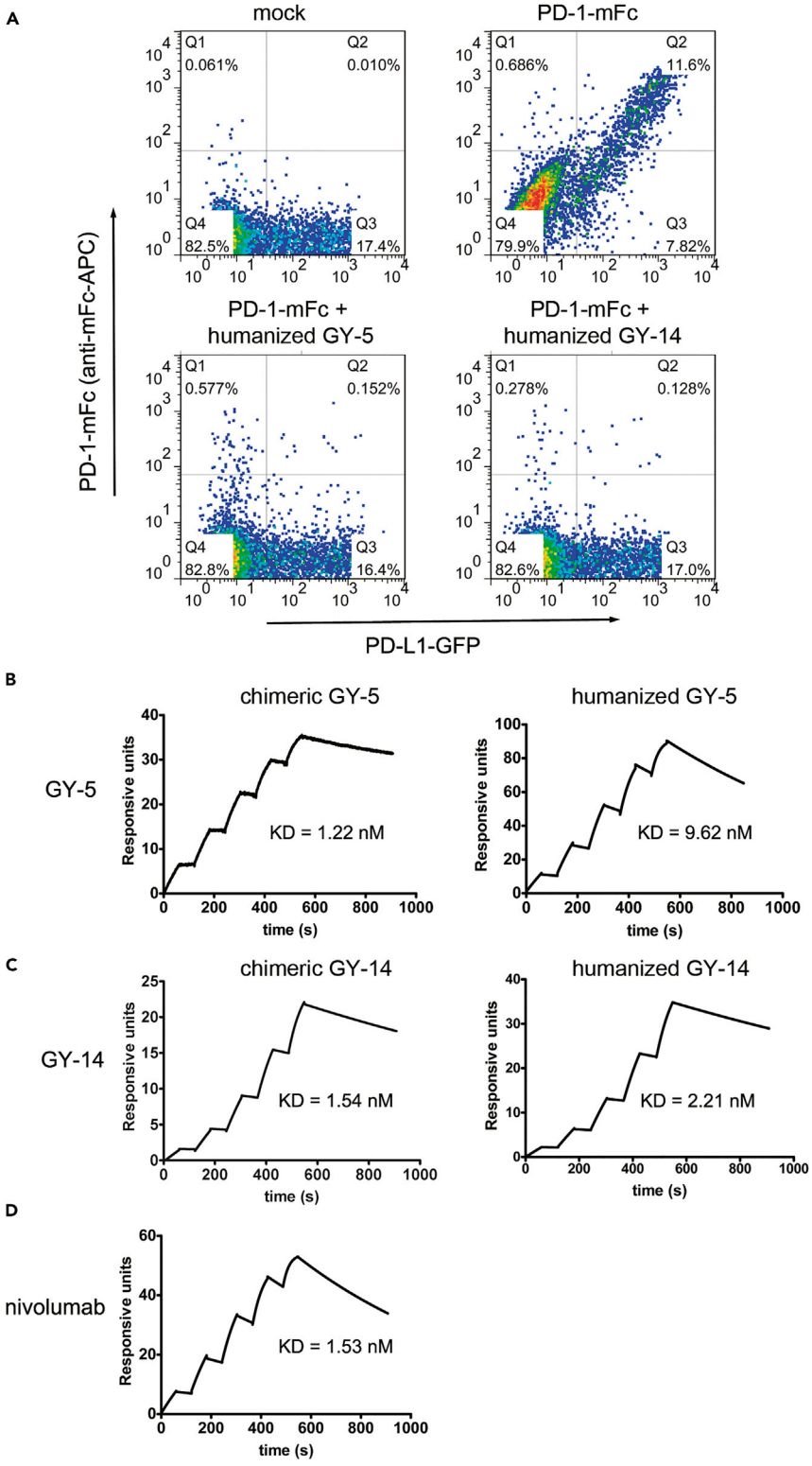

Figure 2. Blocking and Binding Characteristics of Humanized GY-5 and GY-14

(A) The blocking of the binding of PD-1-mFc to PD-L1s expressed on the surface of 293T cells by humanized GY-5 and GY-14 mAbs. The PD-L1-expressing HEK293T cells were stained with PBS and used as negative controls, whereas the staining with PD-1-mFc proteins was used as a positive control. The blocking efficacies of GY-5 and GY-14 were analyzed by

Figure 2. *Continued*

staining of a protein complex of mAbs and PD-1-mFc at a molar ratio of 2:1 and a final concentration of 10 μg/mL. The absence of the PD-1-mFc-staining-positive subpopulation indicates the blockage of the PD-1/PD-L1 interaction.
(B–D) SPR-assay-based characterization of the binding of chimeric and humanized GY-5 (B) or GY-14 (C) to PD-1 was accomplished using a single-cycle BIAcore T100 system. The binding kinetics of nivolumab to PD-1 was evaluated and served as a positive control (D). The equilibrium dissociation constant (K_D) of the binding is labeled accordingly. The data presented here are representatives of two independent experiments with similar results.
See also Figures S3 and S4 and Table S2.

underlies the rationale that blockade of the PD-1 signaling would restore tumor-specific T cell function to eliminate tumor cells (Curiel et al., 2003; Hirano et al., 2005).

Recently, the complex structures of FDA-approved mAbs targeting PD-1 or PD-L1 were determined, providing critical information for our understanding of mAb-based PD-1/PD-L1 blockage for ICT (Tan et al., 2018; Liu et al., 2017; Tan et al., 2016, 2017; Lee et al., 2016; Na et al., 2017). The binding and blocking mechanisms of the two PD-1-targeting mAbs, nivolumab (Opdivo, Bristol-Myers Squibb) and pembrolizumab (Keytruda, Merck) are reported to be quite different (Tan et al., 2016). Nivolumab binds to the N-terminal loop of PD-1, which is outside the Ig-like domain, and competes for the binding of PD-L1 with its light chain (L chain) (Lee et al., 2016; Tan et al., 2017). On the other side, pembrolizumab binds to the C'D loop of PD-1, involving mainly the heavy chain (H chain) of the mAb, and competes with the PD-1/PD-L1 interaction with both its H and L chains (Na et al., 2017). Although the binding regions of nivolumab and pembrolizumab on PD-1 are different, the binding of nivolumab to PD-1 would abrogate the additional binding of pembrolizumab, indicating the competitive binding profiles of these two mAbs (Lee et al., 2016; Tan et al., 2017; Na et al., 2017). However, whether there are "hotspots" for mAb-based anti-PD-1 checkpoint blockage therapy or additional novel "hotspot" regions within PD-1 for therapeutic mAb development remains unknown.

Here, we report the screening of therapeutic mAbs targeting PD-1 and the structural basis of two of these mAbs for PD-1/PD-L1 blockage. We found that the FG loop of PD-1 was targeted by both mAbs, indicating that the PD-1 FG loop may serve as a novel "hotspot" for mAb-based PD-1 ICT. Moreover, the dependency of glycosylation modifications of PD-1 to the binding of these two mAbs was also investigated. Our findings will aid in the future development of biologics or small chemical molecules by targeting PD-1.

RESULTS

Tumor Suppression Efficacy and Humanization of PD-1-Targeting mAbs

To investigate the hotspots on PD-1 for mAbs, B6/C57 mice were vaccinated with human PD-1 protein expressed by HEK293T cells. Thirty one cell hybrid clones that yield PD-1-specific mAbs were obtained after hybridization. Among these mAbs, 23 were found to interrupt the interaction between PD-1 and PD-L1 through a flow cytometry-based assay in which PD-L1 was expressed on 293T cells (Figure S1). Evaluation of the efficiency of enhancing T cell reactivity with enzyme-linked immunospot assays revealed that 11 of the mAbs elevated the T cell responses against influenza A virus M1 peptide pool (Figure S2). Sequences of eight mAb clones were obtained, and the representative GY-5 and GY-14 mAbs were selected for further investigations for their tumor suppressive efficacy and blocking mechanistic studies (Table S1).

Tumor-bearing mouse models were used to investigate anti-tumor activity of chimeric mAbs of GY-5 and GY-14 of human IgG4 subtype. The anti-tumor efficacies of GY-5 and GY-14 were evaluated in the human non-small-cell lung cancer cell line HCC-827-bearing NOD $^{prkdc-/-\ IL-2Rg-/-}$ (NCG) mouse model with pre-established human immunity by inoculation with 1×10^7 peripheral blood mononuclear cells from healthy donors (Figure 1A). An Ebola virus GP-protein-specific mAb, 13C6 (Audet et al., 2014), was used as a negative control. The mAbs were injected intraperitoneally. twice a week for six doses, and tumor volumes were monitored twice a week. The results revealed that both GY-5 and GY-14 showed significant tumor suppression 2 weeks after their first dose compared with 13C6 (Student's t test, $p < 0.05$ or <0.01) (Figure 1).

GY-5 and GY-14 were subsequently humanized via the "CDR grafting" method, and the PD-1/PD-L1 blocking efficiency and binding affinity of the humanized mAbs were evaluated (Figures S3 and S4). Humanized GY-5 and GY-14 could efficiently block the binding of PD-1 to PD-L1s expressed on 293T cells (Figure 2A).

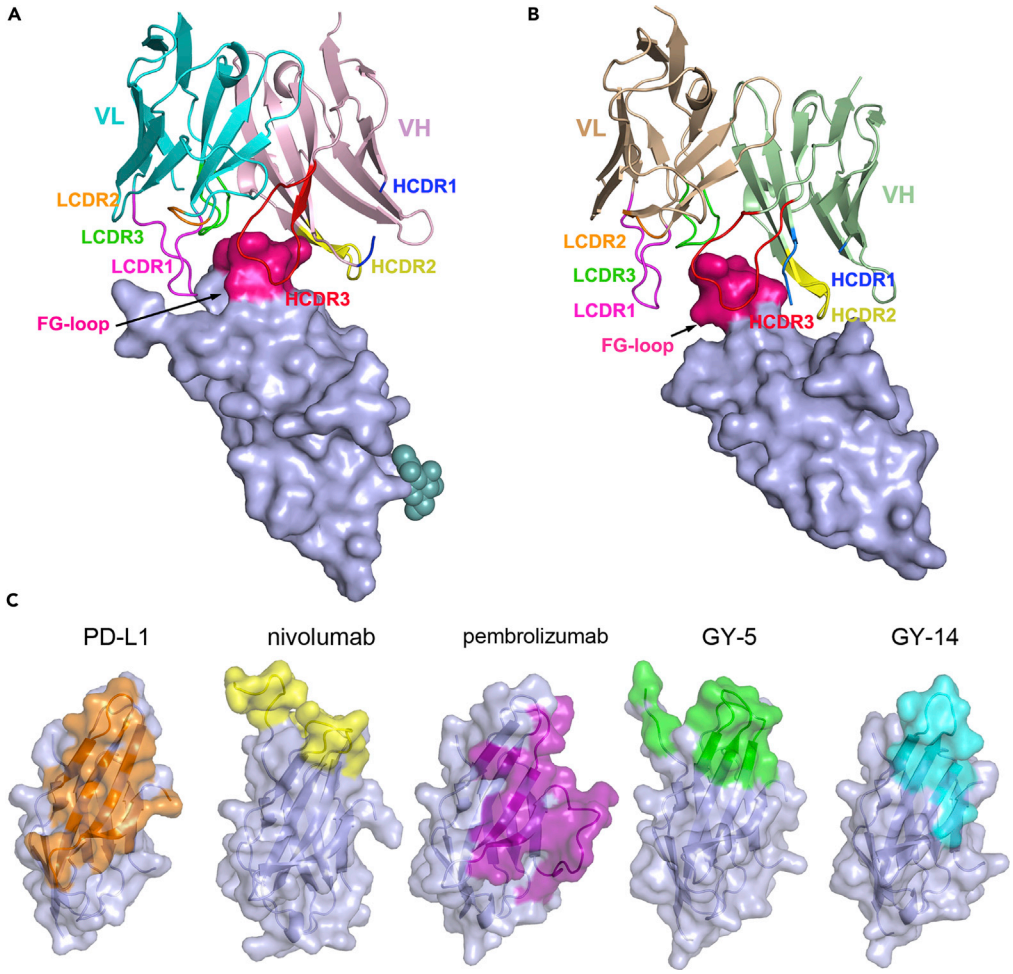

Figure 3. The Complex Structure of GY-5 or GY-14 with PD-1

(A and B) The overall structure of the GY-5 and PD-1 complex (A) or GY-14 and PD-1 complex (B). The V fragments of GY-4 and GY-5 are shown as cartoons, with the heavy chain (VH) and light chain (VL) depicted in different colors, whereas PD-1 is shown in surface representation, and the glycan modifications at N116 are shown as smuggle spheres (light blue). The CDR1, CDR2, and CDR3 loops of the heavy chain (HCDR1, HCDR2, and HCDR3) are colored in blue, yellow, and red, respectively. The CDR1, CDR2, and CDR3 loops of the light chain (LCDR1, LCDR2, and LCDR3) are colored in pink, orange, and green, respectively. The FG loop of the PD-1 molecule is highlighted in hot pink.

(C) Comparison of the binding surface of PD-L1 and complex structures of known PD-1-targeting mAbs on PD-1. The binding surface of PD-L1 and the mAbs targeting PD-1, GY-4, GY-5, nivolumab, and pembrolizumab on PD-1 are presented in orange, green, cyan, yellow, and purple as shown. The PD-1s in the complex with each of the partners were extracted and presented.

See also Table S3.

The binding affinities (K_D) of both chimeric and humanized GY-5 or GY-14 for PD-1 were then analyzed using surface plasmon resonance (SPR) (Figures 2B–2D). We found that the binding affinity of humanized GY-5 and GY-14 (K_D = 9.62 and 2.21 nM, respectively) for PD-1 was similar to that of the chimeric GY-5 and GY-14 mAbs (K_D = 1.22 and 1.54 nM, respectively) (Table S2). Therefore the humanized GY-5 and GY-14 could serve as promising PD-1-targeting therapeutics for tumor ICT.

Structural Basis of GY-5 and GY-14 Binding to PD-1 for PD-1/PD-L1 Blockage

The complex structures of GY-5/PD-1 and GY-14/PD-1 were determined at a resolution of 2.6 and 1.4 Å, respectively, which enabled us to analyze the binding and blocking mechanisms of these two mAbs (Table S3). Overall, GY-5 and GY-14 bind to PD-1 with similar binding orientations, and both mAbs mainly bind to the FG loop of PD-1 (Figures 3A and 3B). The binding of GY-5 mainly involves the CDR2 and CDR3

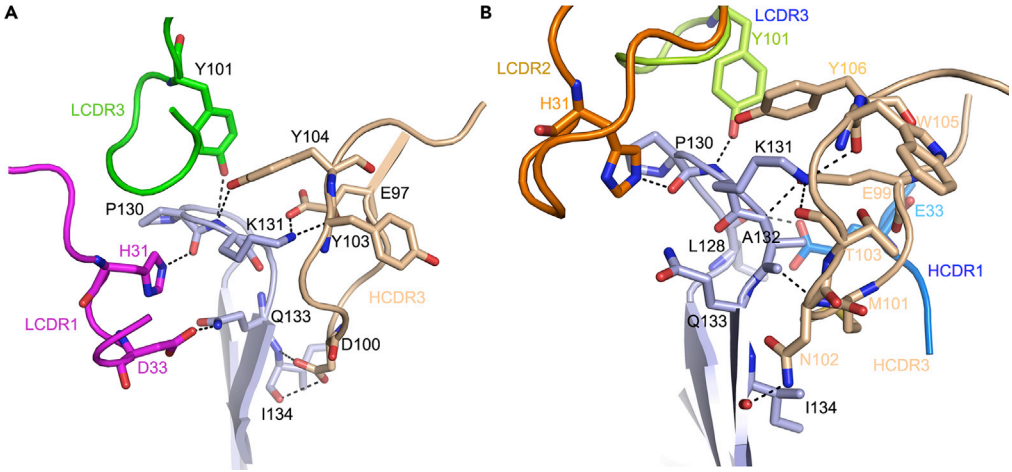

Figure 4. Binding Details of GY-5 and GY-14 to the FG Loop of PD-1

The amino acids forming hydrogen bond interactions between GY-5 and the FG loop of PD-1 (A) or GY-14 and the FG loop (B) are presented as sticks. The LCDR3 and LCDR1 of GY-5 are colored in green and purple, respectively, whereas the HCDR3 of GY-5 and the FG loop of PD-1 are presented in wheat and light blue. The CDRs of GY-14 are colored the same as that of GY-5. The hydrogen bonds are shown as black dashed lines. See also Tables S4 and S5.

of its H chain, and CDR1 and CDR3 of its L chain, with a buried surface of 1,730.1 Å^2 (Figure 3A and Table S4). On the other side, GY-14 utilizes all six CDRs of both the H and L chains to contact PD-1, with a buried surface of 1,602.6 Å^2 (Figure 3B and Table S5). The previously reported complex structures of PD-1/PD-L1, nivolumab/PD-1, and pembrolizumab/PD-1 enabled us to comprehensively compare the binding surface of these mAbs and the ligand (Figure 3C). Nivolumab mainly binds to the N-terminal loop of PD-1, with partial contacts with the FG loop, whereas pembrolizumab mainly binds to the C'D loop. Both GY-5 and GY-14 mainly bind to the FG loop of PD-1, with the binding surfaces of GY-5 and GY-14 being more proximal to that of nivolumab.

Detailed analysis shows that the FG loop of PD-1 contributes major hydrogen bond interactions with GY-5 and GY-14 (Figure 4). Specifically, amino acids of the FG loop (P130, K131, Q133, and I134) formed multiple hydrogen bond interactions with HCDR3 (E97, D100, Y103, and Y104), LCDR1 (H31 and D33), and LCDR3 (Y101) of GY-5 (Figure 4A). Similarly, amino acids of the FG loop (L128, P130, K131, A132, Q133, and I134) formed multiple hydrogen bond interactions with HCDR1 (E33), HCDR3 (E99, M101, N102, T103, W105, and Y106), LCDR2 (H31), and LCDR3 (Y101) of GY-14 (Figure 4B).

We next analyzed the blocking mechanisms of GY-5 and GY-14 to the PD-1/PD-L1 interaction by superimposition of the structure of the previously reported PD-1/PD-L1 complex (PDB code: 4ZQK) with the GY-5/PD-1 complex or GY-14/PD-1 complex, individually (Figure 5). These analyses revealed that the binding of GY-5 and GY-14 induced stereospecific hindrance involving both their H chains to interrupt the binding of PD-L1 to PD-1 (Figures 5A and 5B). The amino acids of the FG loop (L128-Q132) display competitive binding to PD-L1 by both GY-5 and GY-14 (Figures 5C and 5D). However, the competitive binding surfaces of GY-5 and GY-14 are substantially different from each other. These findings suggest that GY-5 and GY-14 bind to PD-1 with similar binding and blocking modes, which is distinct from that of nivolumab and pembrolizumab. In addition, the overwhelming binding affinity of GY-5 or GY-14 (K_D = 1.22 and 1.54 nM, respectively) for PD-1 over PD-L1 (K_D = 0.7–8.3 μM) also ensures the binding priority of the mAbs (Tan et al., 2017). Taken together, the blockade binding mechanism of GY-5 and GY-14 lies in both the overwhelming binding affinity and H-chain-induced stereo-hindrance to the binding of PD-L1 to PD-1.

Glycosylation-Independent Binding of GY-5 and GY-14

PD-1 has four potential N-linked glycosylation sites (N49, N58, N74, and N116) in its IgV domain. We previously reported the N-linked glycosylation modifications at N58, which consist of two N-acetylglucosamines (NAG) and one fucose, for which the protein was prepared from mammalian cells (Tan et al., 2017). In the present structure of PD-1 from the GY-5/PD-1 complex, which was expressed in insect cells, N-linked glycan modifications were visible in three of the four potential N-linked glycosylation sites: N49, N58,

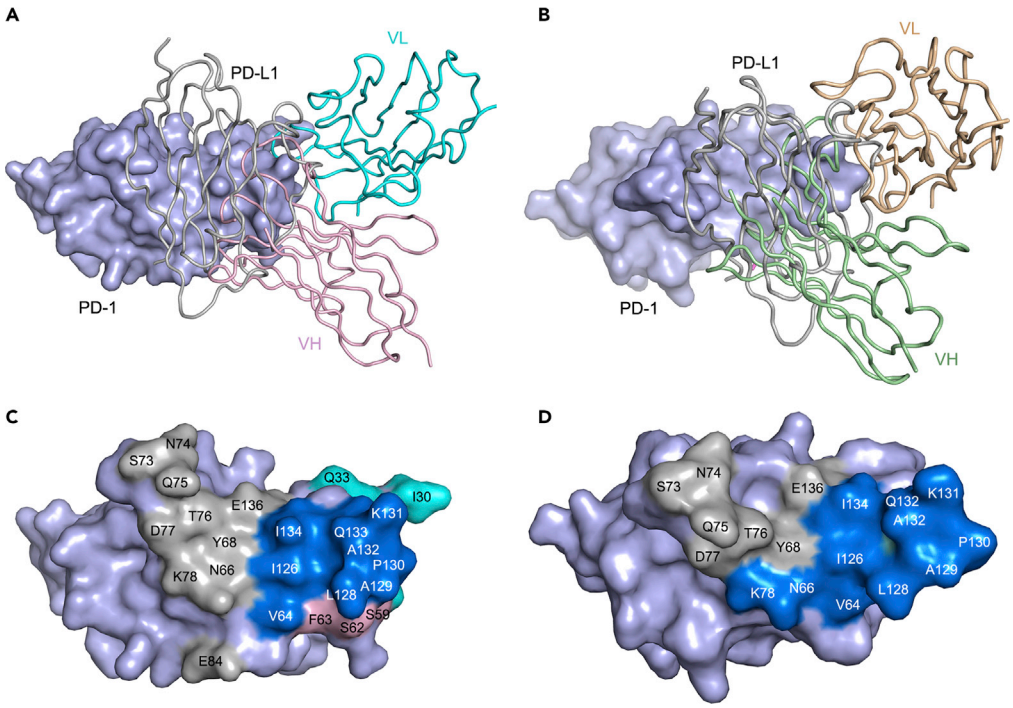

Figure 5. Structural Basis of the Competitive Binding of GY-5 and GY-14 with PD-L1

(A and B) Superimposition of the GY-5/PD-1 complex structure (A) or GY-14/PD-1 complex structure (B) with the PD-1/PD-L1 complex structure (PDB code: 4ZQK). PD-L1 is shown in ribbon format in gray, whereas PD-1 is depicted in surface format in light blue. The VH of GY-5 is depicted as a ribbon in light pink and the VL in cyan, whereas the VH of GY-14 is colored in lemon and VL in wheat.

(C and D) Competitive binding surfaces of GY-5 (C) and GY-14 (D) with PD-L1 on PD-1. The residues in contact with PD-L1 alone are colored in gray, whereas the overlapping residues bound by both PD-L1 and GY-5 (C) or GY-14 (D) are colored in marine. The residues in contact with VH and VL of GY-5 alone are colored in light pink and cyan, respectively. The amino acids in PD-1 which contact with the mAbs or PD-L1 were labeled.

and N116 (Figure 6A). The glycosylation modification at N58 is similar to that observed previously, whereas only a NAG was visible at N49 and N116 (Figures 6B–6D). Considering the flexibility of the glycan chains, N49 and N116 may have more complicated glycan modifications, which is also possible for N74.

The glycosylation may play a role in the folding and function of PD-1 and may further affect the binding of these mAbs (Pinho and Reis, 2015). Therefore we analyzed the binding of GY-5 and GY-14 to PD-1 proteins obtained from the insect cell expression system, which enables partial glycosylation of PD-1 compared with the HEK293T cell expression system, or PD-1 proteins refolded from inclusion bodies expressed in *E. coli* cells as previsouly described (Li et al., 2005; Tan et al., 2017), which have no glycosylation modifications at all. The binding characteristics of these two mAbs were further investigated with SPR analysis. Similar to the glycosylation-independent binding of nivolumab to PD-1, the binding affinity of GY-5 and GY-14 to PD-1 proteins obtained from insect cells (K_D = 1.64 nM and 0.52 nM, respectively) or *E. coli* (K_D = 3.52 and 0.34 nM, respectively) showed no substantial differences from those of PD-1 proteins from 293T cells (Figures 2B, 2C, and 6A and, Table S2). These results indicate that the binding of both GY-5 and GY-14 to PD-1 is independent of PD-1 glycosylation.

The FG Loop of PD-1 Serves as a Novel "Hotspot" for PD-1-Targeting mAbs

To investigate the conformational variations of PD-1 upon binding to different mAbs, the PD-1 structures extracted from the GY-5/PD-1 and GY-14/PD-1 complexes and the other two structurally known nivolumab/PD-1 and pembrolizumab/PD-1 complexes were superimposed. The fold motif of the extracellular PD-1 consists of two β-sheets with multiple strands, together with multiple connecting loops (Figure 7A). Superimposition of the structure of PD-1 from the GY-5/PD-1 complex and GY-14/PD-1 complex yields a root-mean-square deviation of 0.509 Å for 85 Cα pairs, demonstrating the conformational conservation of the

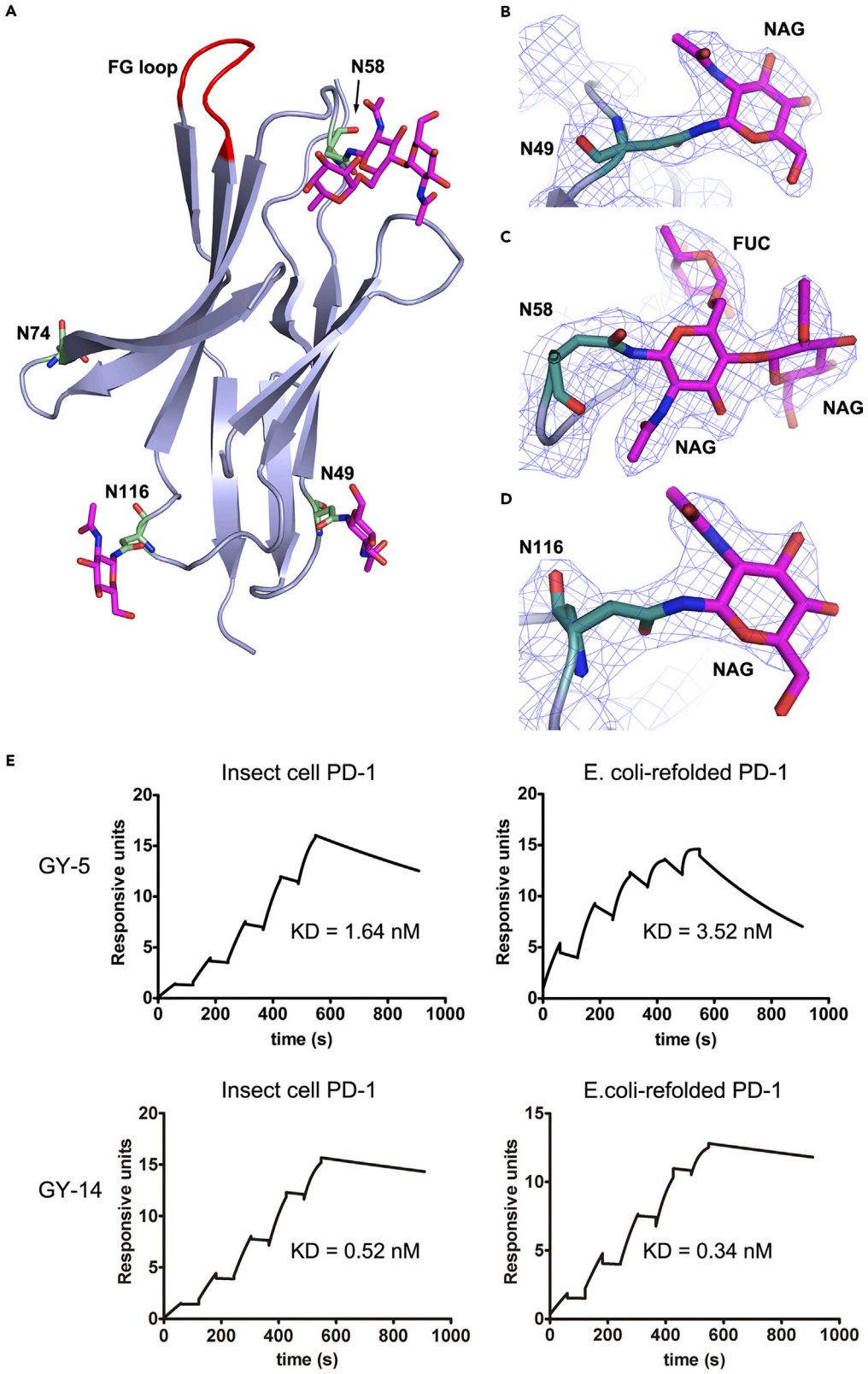
A
FG loop
N58
N74
N116
N49
B
NAG
N49
C
FUC
N58
NAG
NAG
D
N116
NAG
E
Insect cell PD-1
E. coli-refolded PD-1
GY-5
Responsive units
KD = 1.64 nM
KD = 3.52 nM
time (s)
Insect cell PD-1
E.coli-refolded PD-1
GY-14
KD = 0.52 nM
KD = 0.34 nM

Figure 6. Glycosylation Modifications of PD-1 and Glycosylation-Independent Binding of GY-5 and GY-14

(A) Structure of PD-1 with glycans depicted as sticks in purple, and the FG loop is colored in red. Four potential glycosylation sites, N49, N58, N74, and N116, are shown as sticks in light teal.

(B–D) The 2 Fo-Fc electron density maps of N-linked glycans contoured at 1.0 sigma at N49, N58, and N116 are represented in blue. Only one N-acetylglucosamine (NAG) was visible at N49 and N116 (B and D). (C) Three glycans consisting of two NAGs and one L-fucose (FUC) can be clearly observed at N58.

(E) SPR assay characterization of the binding of GY-5 and GY-14 to PD-1 proteins obtained from different expression systems, which enabled varied levels of glycosylation, using a BIAcore T100 system. The refolded PD-1 protein (L25-R147), which was expressed in *E. coli* and refolded *in vitro*, and PD-1 protein obtained from insect cells were analyzed for binding affinity with GY-5 and GY-14, with the mAbs immobilized on the chip. The binding affinity (K_D) is labeled accordingly. The data presented here are a representative of three independent experiments with similar results.

See also Figure S5 and Table S2.

PD-1 proteins upon binding to different mAbs. Although the β-sheet cores of the PD-1s are highly conserved upon binding to different mAbs, the loops connecting the β-strands exhibit substantial conformational variations (Figure 7B). Three loops of PD-1 are targeted in the interaction with therapeutic mAbs, the C′D loop (pembrolizumab), the N-terminal loop (nivolumab), and the FG loop (GY-5 and GY-14) (Figure 7B). The C′D and the N-terminal loops are visible only upon binding to pembrolizumab and nivolumab, respectively, suggesting the high flexibility of these loops. Taken together, the loops of PD-1 are more prone to be targeted and serve as "hotspots" for therapeutic mAb binding.

Partial contacts to the N-terminal loop of PD-1 by GY-5 could be observed, and the influence of this N-terminal loop to the binding affinity of GY-5 was evaluated with an N-terminally truncated PD-1 protein (N32-R147) using SPR (Figure S5). No substantial difference in the binding affinity of GY-5 for the N-terminally truncated PD-1 (N32-R147) (K_D = 11.5 nM) or PD-1 with the N-terminal loop (L25-R147) (K_D = 3.52 nM) was observed. This finding suggests that although the N-terminal loop of PD-1 provides contacts with GY-5, the binding affinity of GY-5 to PD-1 is not affected by the N-terminal loop, which is distinct from the N-terminal loop-dependent binding of nivolumab (Tan et al., 2017).

We further compared the FG loops derived from multiple complex structures to investigate the conformational changes of the FG loop upon binding to different counterparts (Figure 7C). The FG loop of PD-1 contributed partial interaction to the binding of nivolumab, whereas no direct interaction was involved when PD-1 bound to pembrolizumab. The invisibility of the FG loop upon binding to pembrolizumab suggests that this loop has high conformational flexibility. The FG loop of PD-1 upon binding to GY-14 exhibits similar conformation to PD-1 bound to PD-L1 and that of the apo-PD-1. However, a substantial shift of 10.3 Å was observed in the FG loop upon binding to nivolumab or GY-5. Taken together, the FG loop of PD-1 adopts substantially different conformations to bind to varied counterparts, either serving as a major target for mAb binding (e.g., GY-5 and GY-14) or providing partial contacts with mAbs (e.g., nivolumab) or its ligand.

DISCUSSION

In the present study, we report two PD-1-specific mAbs, GY-5 and GY-14, with potent tumor suppressive efficacy. PD-1 contains a front β-sheet face comprising the CC′FG strands and a back β-sheet face comprising the AA′BDE strands. The binding of PD-1 to PD-L1 involves the front β-sheet faces of both molecules, with additional contributions of the FG loop. Structural analysis revealed that both GY-5 and GY-14 mainly bind to the FG loop of PD-1. Together with the previously reported complex structures of nivolumab/PD-1 and pembrolizumab/PD-1, the binding of the four mAbs targeting PD-1 exhibits "loop-dominated" binding characteristics, which is different from PD-L1 binding. The highly flexible loops of PD-1 adopt different conformations when binding to these mAbs. The binding of nivolumab mainly involves the N-terminal loop, whereas pembrolizumab mainly binds to the C′D loop. Both the N-terminal and the C′D loops of PD-1 are away from the binding interface of PD-1/PD-L1. In contrast, both GY-5 and GY-14 mainly bind to the FG loop of PD-1, which shows varied conformations upon binding to different mAbs or its ligand, PD-L1. In contrast to the loops targeted by nivolumab or pembrolizumab, which are away from the PD-1/PD-L1 binding interface, the FG loop of PD-1 plays critical roles in the interaction with PD-L1 (Lin et al., 2008; Lazar-Molnar et al., 2008). Therefore the blocking of the PD-1/PD-L1 interaction by GY-5 and GY-14 relies on occupancy of the FG loop of PD-1 with overwhelming binding affinity compared with the PD-1/PD-L1 interaction. Although the N-terminal loop of PD-1 exhibits partial contacts with GY-5, the overall binding affinity of GY-5 to PD-1 is not affected, as determined through SPR assays

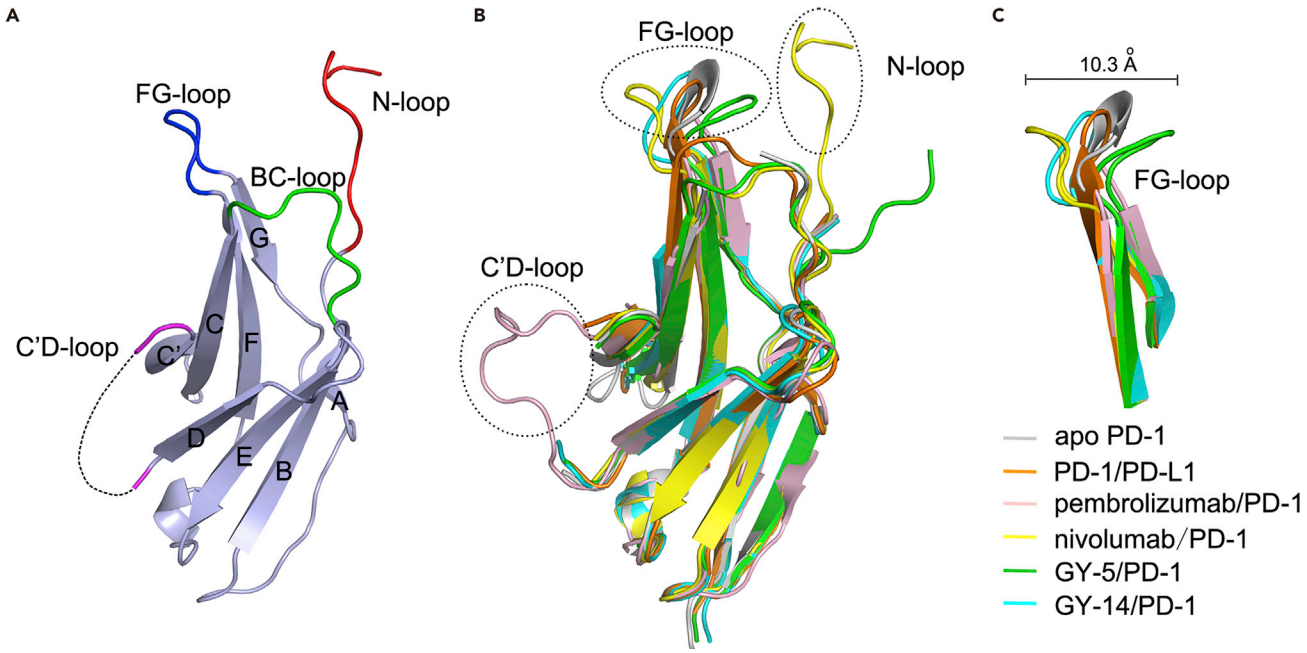

Figure 7. Comparative Binding of PD-1-Targeting mAbs

(A) The location of the loops on PD-1, with the N-terminal loop colored in red, BC loop in green, and FG loop in blue. The invisible C'D loop is depicted as dashed lines in purple.

(B) Superimposition of apo-PD-1 (gray) and the PD-1s extracted from the complex structures of PD-1/PD-L1 (orange) (PDB code: 4ZQK), PD-1/nivolumab (yellow) (PDB code: 5WT9), PD-1/pembrolizumab (light pink) (PDB code: 5JXE), GY-5/PD-1 (green), and GY-14/PD-1 (cyan). The loops that contributed major binding to the mAbs are highlighted in dashed circles.

(C) Comparison of the FG loop of the PD-1s from the complex structures. The FG loop of PD-1 shifted 10.3 Å upon the binding to nivolumab or GY-5.

with an N-terminally loop-truncated PD-1. The FG loop-dominated binding of GY-5 and GY-14 indicates a completely different binding mode from that of nivolumab and pembrolizumab, suggesting that GY-5 and GY-14 are potential therapeutic mAbs in addition to the two commercially available mAbs. Taken together, the FG loop of PD-1 may serve as an important region for the development of PD-1-targeting biologics or small chemical molecules.

Li et al. recently reported that glycosylation of PD-L1 in tumor cells is essential for interaction with PD-1, and an mAb targeting glycosylated PD-L1 would promote PD-L1 internalization and degradation (Li et al., 2018). A wide range of alterations in the glycoproteins on tumor cells can occur, which may correlate with the development and progression of multiple tumors (Pinho and Reis, 2015). Disordered glycosylation modification of the proteins in tumor cells was usually correlated with dysregulated protein folding, trafficking, and protein-protein interactions (Xu and Ng, 2015). In addition to the expression in T cells, PD-1 is also expressed in tumor cells and macrophages, and the expression in these cells may also correlate with the treatment efficacy of PD-1/PD-L1-blocking mAb-based tumor ICT (Kleffel et al., 2015; Gordon et al., 2017; Huang et al., 2009). Therefore investigations of PD-1 glycosylation and the glycan dependency of the interaction of PD-1 with these mAbs would be valuable for our understanding of immune checkpoint blockade therapy (Tan et al., 2017).

PD-1 has four potential N-linked glycosylation sites, and mutational analysis indicates glycosylation modifications at each of these sites (Tan et al., 2017). In the present study, glycosylation modifications were structurally visible at three of the four glycosylation sites: N49, N58, and N116. Considering the flexibility of the glycans, the possibility of glycosylation at N74 cannot be excluded, and more complicated glycan structures may exist at the other three N-linked glycosylation sites. Structural analysis revealed that all these glycosylation sites are located away from PD-1/PD-L1-binding face, suggesting that the glycosylation modifications have no direct influence on the PD-1/PD-L1 interaction. Previous studies reveal that the binding of nivolumab is independent of PD-1 glycosylation, as determined through the analysis of binding affinity to glycosylation-site-mutated PD-1s or PD-1 proteins obtained from different expression systems that

enable different levels of glycosylation of PD-1 (Tan et al., 2017). Although pembrolizumab binds to different regions compared with nivolumab, the structural analysis reveals that the N-linked glycosylation sites are also located away from the pembrolizumab/PD-1 interface (Na et al., 2017). The structural analysis and binding assays of GY-5 and GY-14 to PD-1 proteins obtained from different expression systems demonstrated that the binding of GY-5 and GY-14 is also independent of PD-1 glycosylation. Therefore the FG loop-targeting mAbs may be promising therapeutics independent of dysregulated glycosylation modifications of PD-1 in both immune and tumor cells.

Taken together, we identified two PD-1/PD-L1 blocking mAbs targeting PD-1 with tumor suppressive efficacy. These two mAbs mainly bind to the FG loop of PD-1, which is distinct from the other structurally clear anti-PD-1 mAbs. Glycosylation modifications could be observed at three N-linked glycosylation sites, but the glycosylation modifications were not involved in the binding of these two mAbs to PD-1. These findings have broadened our understanding of mAb-based ICT and will aid in the future development of therapeutics by targeting PD-1.

Limitations of the Study

We do not know the functional anti-tumor advantage of the two mAbs identified in the present study over commercially available PD-1-targeting mAbs. Moreover, there are more PD-1-specific mAbs under clinical investigations and the binding regions of these mAbs on PD-1 may be different from the currently known binding epitopes. Especially, the N58 glycosylation is near the PD-1/PD-L1-binding interface, and future studies should take considerations whether this glycosylation would affect the binding of the mAb.

METHODS

All methods can be found in the accompanying Transparent Methods supplemental file.

DATA AND SOFTWARE AVAILABILITY

The accession number for the atomic coordinates of GY-5/PD-1 complex and GY-14/PD-1 complex reported in this paper is PDB: 6J15 and 6J14.

SUPPLEMENTAL INFORMATION

Supplemental Information can be found online at https://doi.org/10.1016/j.isci.2019.03.017.

ACKNOWLEDGMENTS

This work was supported by Strategic Priority Research Program of Chinese Academy of Sciences (CAS) (XDA12020358 and XDB29040201) and National Science and Technology Major Project (2018ZX09711003-002-001). G.F.G. and J.Y. are supported by the NSFC Innovative Research Group (81621091).

We thank the staff of BL17U and BL19U beamline at the Shanghai Synchrotron Radiation Facility for assistance with data collection. We also thank Yuanyuan Chen, Bingxue Zhou, and Zhenwei Yang from the Institute of Biophysics, CAS, for their technical support in the SPR assay.

AUTHOR CONTRIBUTIONS

G.F.G., J.Y., and S.T. designed and supervised the study. D.C., H.Z, H.W., S.T., R.S., and Z.T. conducted the experiments. Y.C. and J.Q. collected the datasets and solved the structures. S.T., D.C., W.H., J.Z., H.C., S.G., M.X., J.Y., and G.F.G. analyzed the data and wrote the manuscript.

DECLARATION OF INTERESTS

The authors declare no competing interests.

Received: January 9, 2019
Revised: February 27, 2019
Accepted: March 16, 2019
Published: April 26, 2019

REFERENCES

Audet, J., Wong, G., Wang, H., Lu, G., Gao, G.F., Kobinger, G., and Qiu, X. (2014). Molecular characterization of the monoclonal antibodies composing ZMAb: a protective cocktail against ebola virus. Sci. Rep. *4*, 6881.

Apolo, A.B., Infante, J.R., Balmanoukian, A., Patel, M.R., Wang, D., Kelly, K., Mega, A.E., Britten, C.D., Ravaud, A., Mita, A.C., et al. (2017). Avelumab, an anti-programmed death-ligand 1 antibody, in patients with refractory metastatic urothelial carcinoma: results from a multicenter, phase Ib study. J. Clin. Oncol. *35*, 2117–2124.

Balar, A., Bellmunt, J., O'Donnell, P.H., Castellano, D., Grivas, P., Vuky, J., Powles, T., Plimack, E.R., Hahn, N.M., de Wit, R., et al. (2016). Pembrolizumab (pembro) as first-line therapy for advanced/unresectable or metastatic urothelial cancer: preliminary results from the phase 2 KEYNOTE-052 study. Ann. Oncol. *27*, 552–587.

Curiel, T.J., Wei, S., Dong, H., Alvarez, X., Cheng, P., Mottram, P., Krzysiek, R., Knutson, K.L., Daniel, B., Zimmermann, M.C., et al. (2003). Blockade of B7-H1 improves myeloid dendritic cell-mediated antitumor immunity. Nat. Med. *9*, 562–567.

Callahan, M.K., Postow, M.A., and Wolchok, J.D. (2016). Targeting T cell co-receptors for cancer therapy. Immunity *44*, 1069–1078.

Freeman, G.J., Long, A.J., Iwai, Y., Bourque, K., Chernova, T., Nishimura, H., Fitz, L.J., Malenkovich, N., Okazaki, T., Byrne, M.C., et al. (2000). Engagement of the PD-1 immunoinhibitory receptor by a novel B7 family member leads to negative regulation of lymphocyte activation. J. Exp. Med. *192*, 1027–1110.34.

Gridelli, C., Ardizzoni, A., Barberis, M., Cappuzzo, F., Casaluce, F., Danesi, R., Troncone, G., and De Marinis, F. (2017). Predictive biomarkers of immunotherapy for non-small cell lung cancer: results from an Experts Panel Meeting of the Italian Association of Thoracic Oncology. Transl. Lung Cancer Res. *6*, 373–386.

Gordon, S.R., Maute, R.L., Dulken, B.W., Hutter, G., George, B.M., McCracken, M.N., Gupta, R., Tsai, J.M., Sinha, R., Corey, D., et al. (2017). PD-1 expression by tumour-associated macrophages inhibits phagocytosis and tumour immunity. Nature *545*, 495–499.

He, M., Chai, Y., Qi, J., Zhang, C.W., Tong, Z., Shi, Y., Yan, J., Tan, S., and Gao, G.F. (2017). Remarkably similar CTLA-4 binding properties of therapeutic ipilimumab and tremelimumab antibodies. Oncotarget *8*, 67129–67139.

Hirano, F., Kaneko, K., Tamura, H., Dong, H., Wang, S., Ichikawa, M., Rietz, C., Flies, D.B., Lau, J.S., Zhu, G., et al. (2005). Blockade of B7-H1 and PD-1 by monoclonal antibodies potentiates cancer therapeutic immunity. Cancer Res. *65*, 1089–1096.

Huang, X., Venet, F., Wang, Y.L., Lepape, A., Yuan, Z., Chen, Y., Swan, R., Kherouf, H., Monneret, G., Chung, C.S., et al. (2009). PD-1 expression by macrophages plays a pathologic role in altering microbial clearance and the innate inflammatory response to sepsis. Proc. Natl. Acad. Sci. U S A *106*, 6303–6308.

Ishida, Y., Agata, Y., Shibahara, K., and Honjo, T. (1992). Induced expression of PD-1, a novel member of the immunoglobulin gene superfamily, upon programmed cell death. EMBO J. *11*, 3887–3895.

Iwai, Y., Ishida, M., Tanaka, Y., Okazaki, T., Honjo, T., and Minato, N. (2002). Involvement of PD-L1 on tumor cells in the escape from host immune system and tumor immunotherapy by PD-L1 blockade. Proc. Natl. Acad. Sci. U S A *99*, 12293–12297.

Kleffel, S., Posch, C., Barthel, S.R., Mueller, H., Schlapbach, C., Guenova, E., Elco, C.P., Lee, N., Juneja, V.R., Zhan, Q., et al. (2015). Melanoma cell-intrinsic PD-1 receptor functions promote tumor growth. Cell *162*, 1242–1256.

Latchman, Y., Wood, C.R., Chernova, T., Chaudhary, D., Borde, M., Chernova, I., Iwai, Y., Long, A.J., Brown, J.A., Nunes, R., et al. (2001). PD-L2 is a second ligand for PD-1 and inhibits T cell activation. Nat. Immunol. *2*, 261–268.

Lazar-Molnar, E., Yan, Q., Cao, E., Ramagopal, U., Nathenson, S.G., and Almo, S.C. (2008). Crystal structure of the complex between programmed death-1 (PD-1) and its ligand PD-L2. Proc. Natl. Acad. Sci. U S A *105*, 10483–10488.

Lee, J.Y., Lee, H.T., Shin, W., Chae, J., Choi, J., Kim, S.H., Lim, H., Won Heo, T., Park, K.Y., Lee, Y.J., et al. (2016). Structural basis of checkpoint blockade by monoclonal antibodies in cancer immunotherapy. Nat. Commun. *7*, 13354.

Li, C.W., Lim, S.O., Chung, E.M., Kim, Y.S., Park, A.H., Yao, J., Cha, J.H., Xia, W., Chan, L.C., Kim, T., et al. (2018). Eradication of triple-negative breast cancer cells by targeting glycosylated PD-L1. Cancer Cell *33*, 187–201.e10.

Li, H., Zhou, M., Han, J., Zhu, X., Dong, T., Gao, G.F., and Tien, P. (2005). Generation of murine CTL by a hepatitis B virus-specific peptide and evaluation of the adjuvant effect of heat shock protein glycoprotein 96 and its terminal fragments. J. Immunol. *174*, 195–204.

Lin, D.Y., Tanaka, Y., Iwasaki, M., Gittis, A.G., Su, H.P., Mikami, B., Okazaki, T., Honjo, T., Minato, N., and Garboczi, D.N. (2008). The PD-1/PD-L1 complex resembles the antigen-binding Fv domains of antibodies and T cell receptors. Proc. Natl. Acad. Sci. U S A *105*, 3011–3016.

Liu, K., Tan, S., Chai, Y., Chen, D., Song, H., Zhang, C.W., Shi, Y., Liu, J., Tan, W., Lyu, J., et al. (2017). Structural basis of anti-PD-L1 monoclonal antibody avelumab for tumor therapy. Cell Res. *27*, 151–153.

Massard, C., Gordon, M.S., Sharma, S., Rafii, S., Wainberg, Z.A., Luke, J., Curiel, T.J., Colon-Otero, G., Hamid, O., Sanborn, R.E., et al. (2016). Safety and efficacy of durvalumab (MEDI4736), an anti-programmed cell death ligand-1 immune checkpoint inhibitor, in patients with advanced urothelial bladder cancer. J. Clin. Oncol. *34*, 3119–3125.

Motzer, R.J., Escudier, B., McDermott, D.F., George, S., Hammers, H.J., Srinivas, S., Tykodi, S.S., Sosman, J.A., Procopio, G., Plimack, E.R., et al. (2015). Nivolumab versus Everolimus in advanced renal-cell carcinoma. N. Engl. J. Med. *373*, 1803–1813.

Na, Z., Yeo, S.P., Bharath, S.R., Bowler, M.W., Balikçi, E., Wang, C.I., and Song, H. (2017). Structural basis for blocking PD-1-mediated immune suppression by therapeutic antibody pembrolizumab. Cell Res. *27*, 147–150.

Nishimura, H., Nose, M., Hiai, H., Minato, N., and Honjo, T. (1999). Development of lupus-like autoimmune diseases by disruption of the PD-1 gene encoding an ITIM motif-carrying immunoreceptor. Immunity *11*, 141–151.

Pinho, S.S., and Reis, C.A. (2015). Glycosylation in cancer: mechanisms and clinical implications. Nat. Rev. Cancer *15*, 540–555.

Powles, T., O'Donnell, H., Massard, C., Arkenau, H., Friedlander, T.W., Hoimes, C., Lee, J., Ong, M., Sridhar, S.S., Vogelzang, N.J., et al. (2017). Updated efficacy and tolerability of durvalumab in locally advanced or metastatic urothelial carcinoma. J. Clin. Oncol. *35*, 286.

Robert, C., Schachter, J., Long, G.V., Arance, A., Grob, J.J., Mortier, L., Daud, A., Carlino, M.S., McNeil, C., Lotem, M., et al. (2015). Pembrolizumab versus Ipilimumab in advanced melanoma. N. Engl. J. Med. *372*, 2521–2532.

Tan, S., and Gao, G.F. (2015). New hope for cancer treatment: cancer immunotherapy. Chin. Sci. Bull. *60*, 3155–3157, (in Chinese).

Tan, S., Chen, D., Liu, K., He, M., Song, H., Shi, Y., Liu, J., Zhang, C.W., Qi, J., Yan, J., et al. (2016). Crystal clear: visualizing the intervention mechanism of the PD-1/PD-L1 interaction by two cancer therapeutic monoclonal antibodies. Protein Cell *7*, 866–877.

Tan, S., Zhang, H., Chai, Y., Song, H., Tong, Z., Wang, Q., Qi, J., Wong, G., Zhu, X., Liu, W.J., et al. (2017). An unexpected N-terminal loop in PD-1 dominates binding by nivolumab. Nat. Commun. *8*, 14369.

Tan, S., Liu, K., Chai, Y., Zhang, C.W., Gao, S., Gao, G.F., and Qi, J. (2018). Distinct PD-L1 binding characteristics of therapeutic monoclonal antibody durvalumab. Protein Cell *9*, 135–139.

Topalian, S.L., Hodi, F.S., Brahmer, J.R., Gettinger, S.N., Smith, D.C., McDermott, D.F., Powderly, J.D., Carvajal, R.D., Sosman, J.A., Atkins, M.B., et al. (2012). Safety, activity, and immune correlates of anti-PD-1 antibody in cancer. N. Engl. J. Med. *366*, 2443–2454.

Tumeh, P.C., Harview, C.L., Yearley, J.H., Shintaku, I.P., Taylor, E.J., Robert, L., Chmielowski, B., Spasic, M., Henry, G., Ciobanu, V., et al. (2014). PD-1 blockade induces responses by inhibiting adaptive immune resistance. Nature *515*, 568–571.

Xu, C., and Ng, D.T. (2015). Glycosylation-directed quality control of protein folding. Nat. Rev. Mol. Cell Biol. *16*, 742–752.

ISCI, Volume *14*

Supplemental Information

The FG Loop of PD-1 Serves as a "Hotspot" for Therapeutic Monoclonal Antibodies in Tumor Immune Checkpoint Therapy

Danqing Chen, Shuguang Tan, Hao Zhang, Haiyuan Wang, Weiwu He, Rui Shi, Zhou Tong, Jianhua Zhu, Hao Cheng, Shan Gao, Yan Chai, Jianxun Qi, Minghui Xiao, Jinghua Yan, and George F. Gao

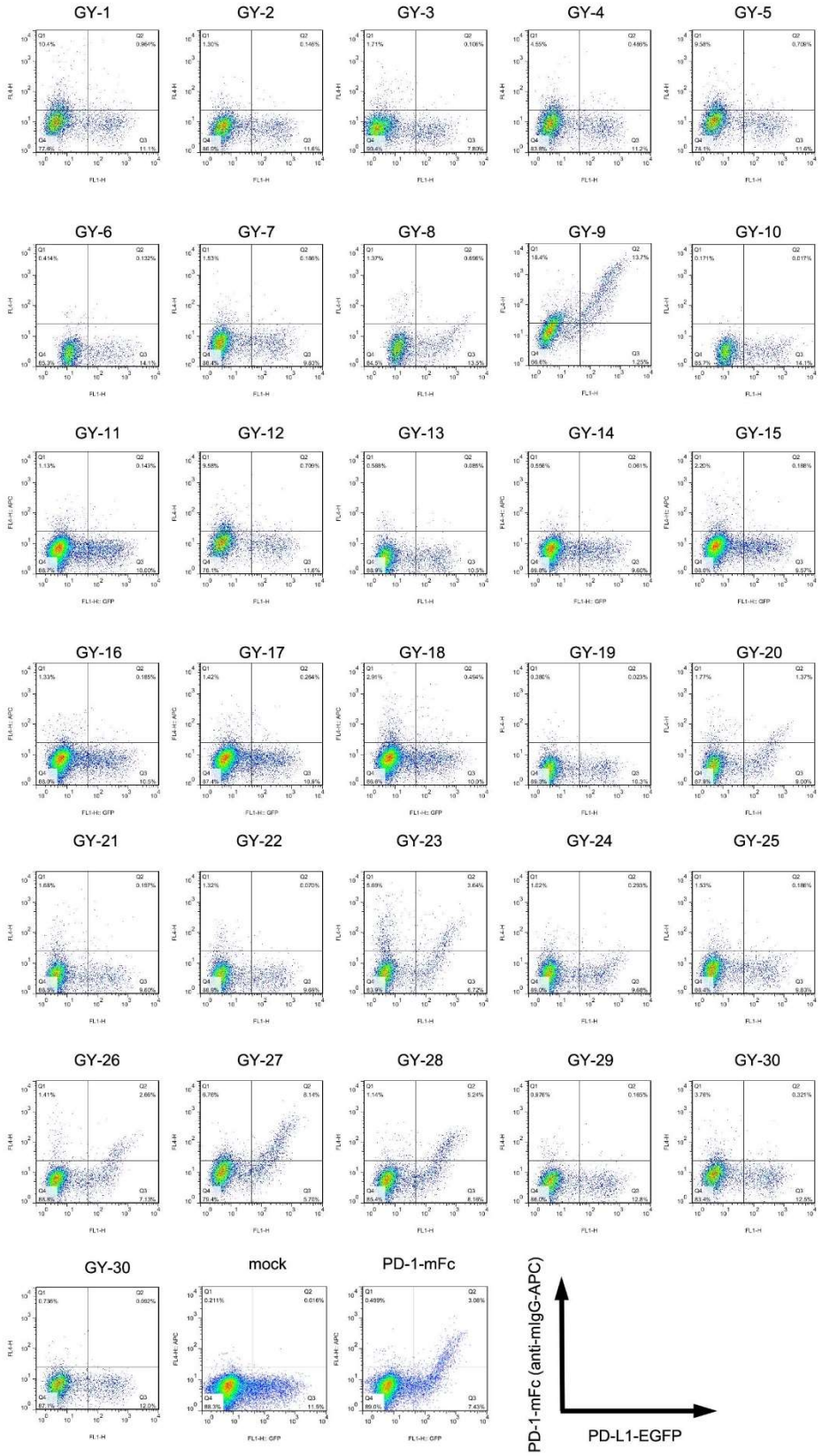

Figure S1. Screening of PD-1/PD-L1 blocking MAbs targeting PD-1, related to Figure 1. The blocking of the binding of PD-1-mFc to PD-L1s expressed on the

surface of 293T cells by MAbs targeting PD-1. The PD-L1 expressing HEK 293T cells were stained with PBS as mock, while the staining with PD-1-mFc proteins was involved as positive control. The blocking efficacy of the MAbs was analyzed by staining of a protein complex of MAbs and PD-1-mFc at a molar ratio of 2:1 and a final concentration of 10 μg/mL. The absence of the PD-1-mFc staining positive subpopulation indicates the blockade of PD-1/PD-L1 interaction. The data presented here is representative of three independent experiments with similar results.

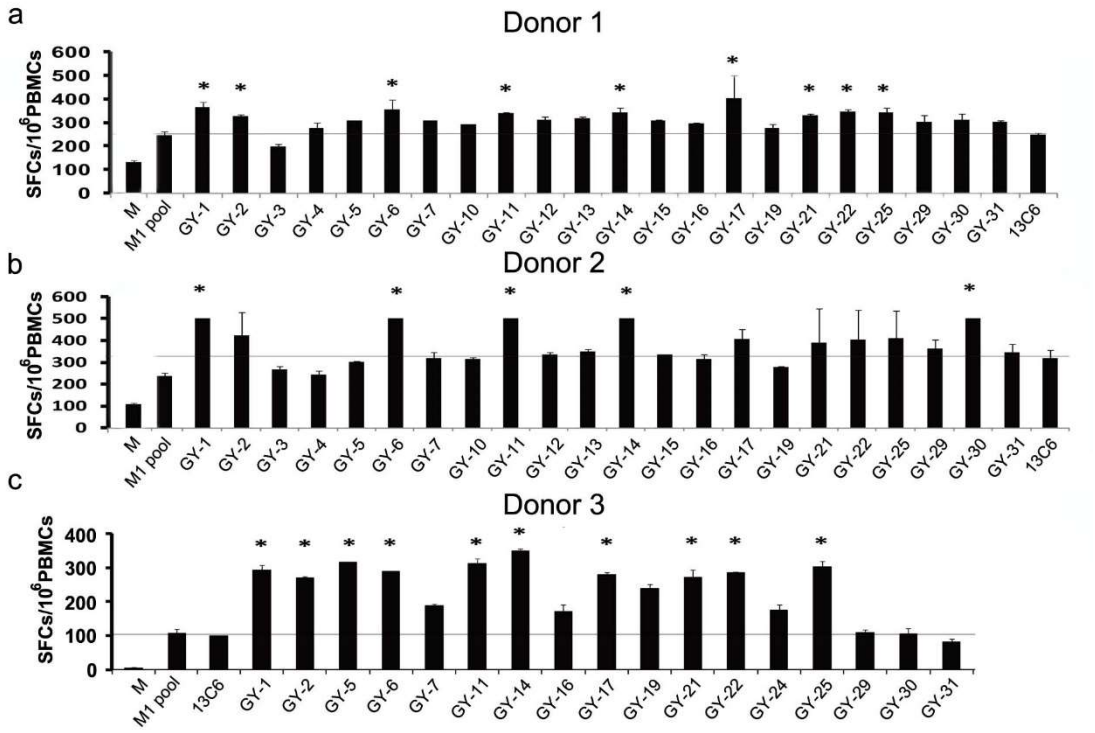

Figure S2. T cell activating efficacy of the MAbs, related to Figure 1. IFN-γ secreting cells were detected with PBMCs from three healthy donors, donor 1, donor 2 and donor 3, stimulated with a peptide pool of M1 of 2009 pN1N1 virus. The activating efficacy of PD-1 specific MAbs to M1 specific T cell responses were evaluated with simultaneous stimulation of the PBMCs with the MAbs and M1 peptide pool. PBMCs incubated with medium alone were enrolled as mock. PBMCs stimulated with M1 peptide pool alone or together with Ebola virus GP protein specific 13C6 MAb were served as negative control. The SE was represented on each MAb bar. *: $p < 0.05$. The data presented here is representative of three independent experiments with similar results.

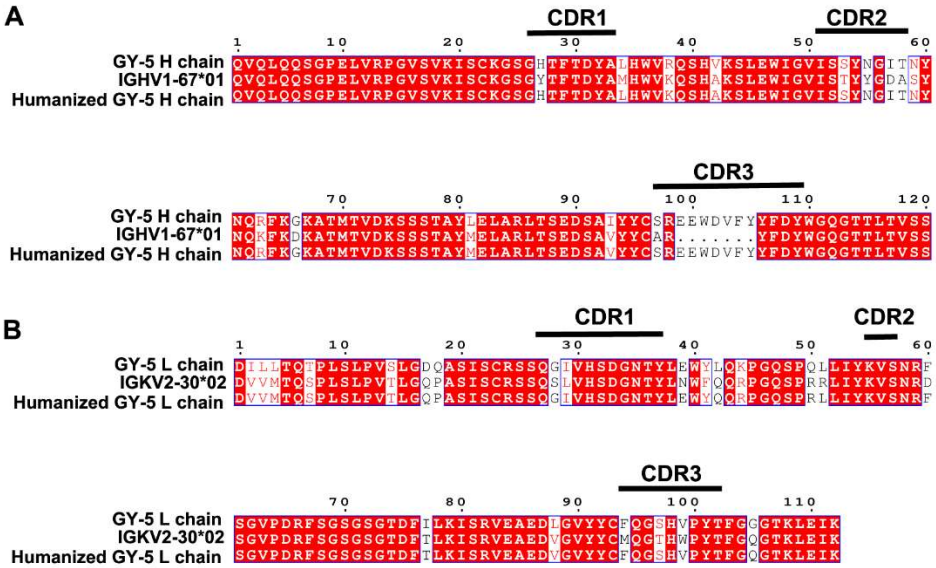

Figure S3. Humanization strategy of GY-5, related to Figure 2. Sequence alignments highlighting the humanization strategy of GY-5 by retaining all the CDRs and substituting the remaining amino acids with the equivalent residues of the human immunoglobulins. The human antibody of IGHV1-67*01, which exhibits the highest sequence identity to GY-5 in heavy chain, was selected as the humanization backbone, while IGKV2-30*02 was selected as the humanization backbone for the light chain.

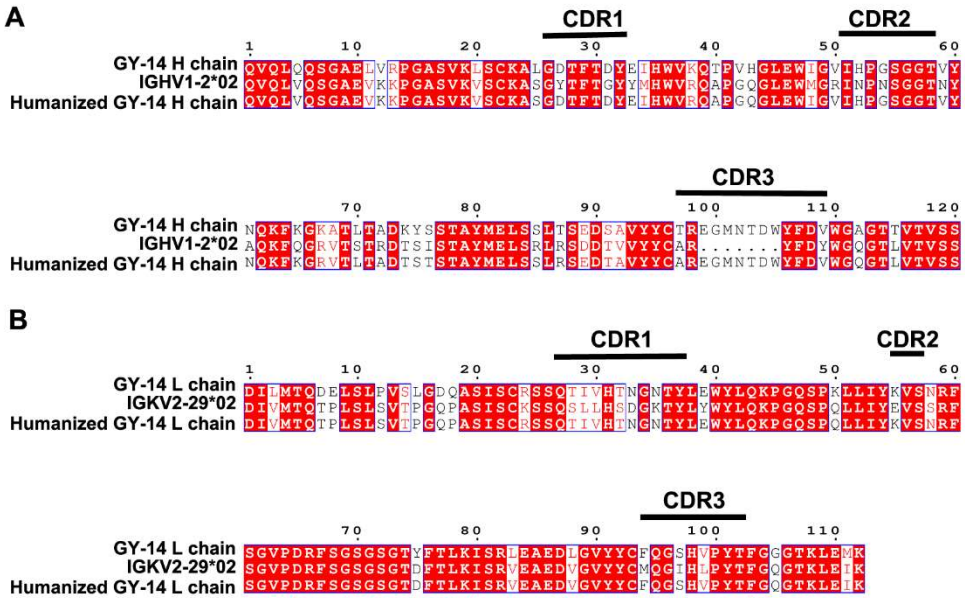

Figure S4. Humanization strategy of GY-14, related to Figure 2. Sequence alignments highlighting the humanization strategy of GY-14 by retaining all the CDRs

and substituting the remaining amino acids with the equivalent residues of the human immunoglobulins. The human antibody of IGHV1-2*02, which exhibits the highest sequence identity to GY-5 in heavy chain, was selected as the humanization backbone, while IGKV2-29*02 was selected as the humanization backbone for the light chain.

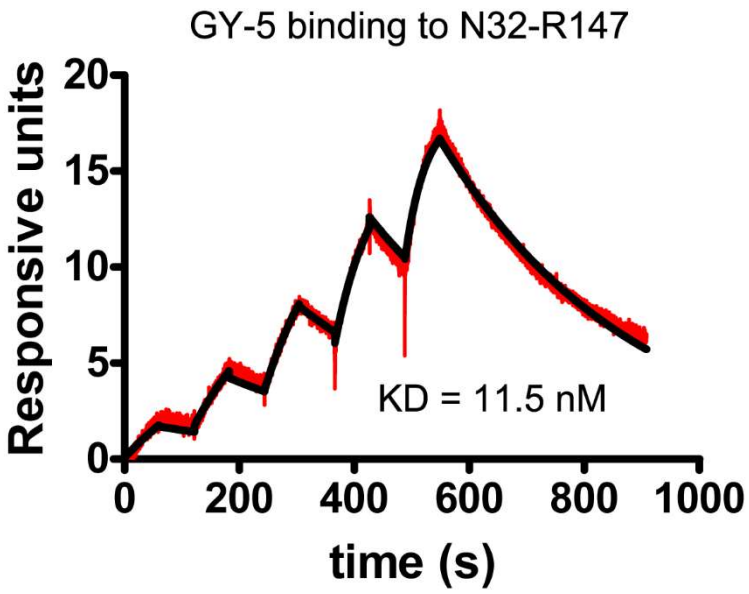

Figure S5. SPR assay-based characterization of the binding of GY-5 to N-terminal truncated PD-1, related to Figure 6. The assay was accomplished using a single-cycle BIAcore® T100 system. The equilibrium dissociation constant (KD) of the binding are labeled accordingly. The fits of the binding curves are shown in red. The data presented here are representative of two independent experiments with similar results.

Table S1. Sequence of the MAbs with T cell activating efficacy, related to Figure 1

MAb	L-V	L-J	LCDR3	H-V allele	H-J	HCDR3
GY-1	KV1-117*01	2*01	QGSHVPYT	HV1-15*01	1*01	TREGMNTDWYDV
GY-2	KV1-117*01	2*01	QGSHVPYT	HV1-67*01	2*01	AREEWDVYYDYW
GY-5	KV1-117*01	2*01	QGSHVPYT	HV1-67*01	2*01	SREEWDVYYDYW
GY-6	KV3-12*01	5*01	QHSWELPLT	HV1-S81*02	2*01	TRRDYRYDGGDY
GY-11	KV3-12*01	5*01	QHSWELPLT	HV1-S81*02	2*01	TRRDYRYDGGYD
GY-14	KV1-117*01	2*01	QGSHVPYT	HV1-15*01	1*01	TREGMNTDWYDV
GY-17	KV1-117*01	2*01	QGSHVPYT	HV1-67*01	2*01	SREEWDVYYDYW
GY-25	KV3-12*01	5*01	QHSWELPLT	HV1-S81*02	2*01	TRRDYRYDGGDY

Table S2. Binding profiles of GY-5 and GY-14 to PD-1, related to Figure 2 and 6

Antibody	PD-1 protein expressing cell	K_a (M •s)[1]	K_d (s)[2]	K_D (nM)
Chimeric GY-5	293T cell	2.13×10^5	2.59×10^{-4}	1.22
Chimeric GY-14	293T cell	3.42×10^5	5.27×10^{-4}	1.54
Humanized GY-5	293T cell	1.13×10^5	10.9×10^{-4}	9.62
Humanized GY-14	293T cell	2.38×10^5	5.26×10^{-4}	2.21
nivolumab	293T cell	8.08×10^5	12.36×10^{-4}	1.53
Chimeric GY-5	Insect cell	4.17×10^5	6.84×10^{-4}	1.64
Chimeric GY-5	*E. coli*	5.41×10^5	19.06×10^{-4}	3.52
Chimeric GY-14	Insect cell	4.81×10^5	2.51×10^{-4}	0.52
Chimeric GY-14	*E. coli*	6.62×10^5	2.26×10^{-4}	0.34

[1] K_a, association rate constant.

[2] K_d, dissociation rate constant.

Table S3. Crystallographic data collection and refinement statistics, related to Figure 3.

	GY-5/PD-1	GY-14/PD-1
Data collection		
Space group	P 1 21 1	P 1 21 1
Wavelength (Å)	0.979	0.978
Unit cell dimensions		
a, *b*, *c* (Å)	61.59, 64.35, 151.48	43.42, 75.68, 55.87
α, β, γ (°)	90.0, 98.04, 90.0	90.0, 104.3, 90.0
Resolution (Å)	50.0-2.60 (2.69-2.60)	50.0-1.40 (1.40-1.45)
No. reflections	33831	66956
R_{merge}	0.109 (0.859)	0.039 (0.222)
I / σ	3.17 (2.61)	7.69 (1.40)
Completeness (%)	92.2	97.07
Redundancy	6.2 (6.5)	7.0 (7.2)
Refinement		
Resolution (Å)	41.6-2.6	44.0- 1.4
R_{work} / R_{free}	0.212/0.276	0.188/0.215
No. atoms		
Protein	8342	2958
Ligands	0	0
Water	0	392
B-factors		
Protein	41.2	13.0
Ligands		
Water		
R.m.s. deviations		
Bond lengths (Å)	0.010	0.007
Bond angles (°)	1.248	0.933
Ramachandran plot		
Favored (%)	95.83	97.12
Allowed (%)	4.17	2.56
Outliers (%)	0.00	0.32

*Values in parentheses are for highest-resolution shell.

Table S4. Interaction between GY-5 and PD-1, related to Figure 4

	GY-5	PD-1	Contacts
H chain	A31	L128, A132	1[1],1
	V48	L128,A129	9,1
	I49	L128	5
	S50	L128	6
	Y52	V64,I126	1, 7
	N53	V64	1
	I55	S62,F63,L128	5,2,6
	T56	S62, L128	4(1)[2],3
	N57	S60, S62, L128, A129	2,7(1),1,4
	E97	K131, A129	13(2),7
	W99	I126,S127, L128, A132,Q133,I134	4,6,6,13,8,4
	D100	A132,Q133,I134	3(1),5,16(1)
	V101	K131	5
	F102	K131	3
	Y103	K131	6(1)
	Y104	P130,K131	1,17(1)
L chain	Y101	L128,A129 P130,K131	1,3,7,4(1)
	V30	I30	3
	H31	I30, P130, K131, Q133	2,10(1),5,6
	S32	I30, W32, T59	3,8,4
	D33	I30, W32, Q133, K135	1,7,4(1),1
	G34	I30	4
	Y37	K131, Q133	15,1
	G96	P130, K131	1,1
	S97	P130	4
	H98	P130	2
	V99	A129, P130	3,6

[1] Numbers represent the number of atom-to-atom contacts between the antibody residues and the hPD-1 residues, which were analyzed by the Contact program in CCP4 suite (the distance cutoff is 4.5Å).

[2] Numbers in the parentheses represent the number of hydrogen bonds between the antibody residues and the hPD-1 residues, which were analyzed by the Contact program in CCP4 suite (the distance cutoff is 3.5 Å).

Table S5. Interaction between GY-14 and PD-1, related to Figure 4

	GY-14	PD-1	Contacts
H chain	T29	Q75	10[1]
	Y32	K78, D85, Q88, P89	6(1) [2], 3, 12, 12
	Y34	S87, P89	6(1), 3
	G49	P89	4
	I50	P89	8
	N51	P89	8
	S53	Q75, D77	4(1), 6(1)
	N54	G90	1
	G56	P89, G90	6, 6
	T57	P89, G90	3, 6
	N58	S87, Q88, P89	4, 4, 14
	R98	K78, D85, S87, Q88	1, 9(2), 8(1), 1
	Y100	T76, D77, K78, D85	11 (1),2,12(1),1
	R101	V64, N66, Y68, K78, I126, I134	1,7(1),4,1,4,2
	Y102	V64, I126, L128	1,3,5
	D103	S87	2
L chain	H31	R86	2
	S32	P83	5
	D33	E61, S62, F63, F82, P83	7,14(1),15,1,3
	G34	S62	6(1)
	N35	P83	2
	Y37	P83, E84, R86	2,1,10
	Y54	L128	2
	K55	L128	1
	N58	L128, A129	5
	G96	R86	3
	S97	R86	12(1)
	Y101	S87	17(2)

[1] Numbers represent the number of atom-to-atom contacts between the antibody residues and the hPD-1 residues, which were analyzed by the Contact program in CCP4 suite (the distance cutoff is 4.5Å).

[2] Numbers in the parentheses represent the number of hydrogen bonds between the antibody residues and the hPD-1 residues, which were analyzed by the Contact program in CCP4 suite (the distance cutoff is 3.5 Å).

Transparent Methods

Ethics statement.

The study was approved by the Research Ethics Committee of Institute of Microbiology, Chinese Academy of Sciences. All of the subjects provided written informed consent for the studies performed on their samples and publication of their cases. Animals used in this study (6-to-8-week-old female NCG mice) were bought from Model Animal Research Center of Nanjing University. The study was conducted in accordance with the principles of the Declaration of Helsinki and the standards of good clinical practice (as defined by the International Conference on Harmonization) , and Chinese regulatory requirements, as stipulated by the Chinese Food and Drug Administration.

Protein expression and purification

Three expression systems, *i.e.*, *E.coli*, insect cell, HEK 293T cell, were used to express PD-1 proteins for crystal screening or binding affinity analysis as previously described (Tan et al., 2017). Two constructs with PD-1 fragment of L25-R147 or N33-R147 (UniProt: Q15116) were cloned into pET21a vector (Invitrogen). The protein was expressed in *E.coli* as inclusion bodies and refolded *in vitro* as described previously (Liu et al., 2017; He et al., 2017; Tan et al., 2018; Li et al., 2015). The construct encoding PD-1 fragment (residue N33-R147) was cloned into pFastbac1 vector (Invitrogen) with an N-terminal gp67 signal peptide and a C-terminal hexa-His tag. Transfection and virus amplification were performed according to the Bac-to-Bac baculovirus expression system manual (Invitrogen). The Hi5 cells (Invitrogen) were

infected by the recombinant baculovirus to produce soluble PD-1. Then the supernatant containing soluble PD-1 was purified by sequentially His-Trap HP column (GE Healthcare) and Superdex® 200 10/300 GL (GE Healthcare) in a 20 mM Tris and 150 mM NaCl (pH 8.0) buffer. The DNA encoding the ectodomain of PD-1 (residues M1-Q147, including signal peptide, UniProt: Q15116) with either a C-terminal hexa-His tag (plasmid PD-1-pCAGGS) or mouse IgG-Fc Fragment at the C terminus (plasmid PD-1-mFc-pCAGGS) were cloned into pCAGGS vector (Addgene) with *EcoR*I and *Bgl*II restriction sites. Plasmid PD-1-pCAGGS or PD-1-mFc-pCAGGS was transiently transfected into HEK 293 T cells (ATCC) for protein expression. The PD-1-mFc protein was purified using a Protein G affinity column (GE Healthcare), while PD-1-his protein was purified by His-Trap HP column (GE Healthcare). PD-1-mFc protein or PD-1-his protein was subsequently purified by gel filtration on a Superdex 200 10/300 GL (GE Healthcare) in a buffer containing 20 mM Tris (pH 8.0) and 150 mM NaCl.

The mouse ascites fluid with GY-5 was diluted with an equal volume of 20 mM Na_3PO_4 (pH 7.0) buffer and filtered through a 0.22 μm filter (Millipore). The antibodies were purified on a Protein G affinity column. GY-5 Fab fragments were obtained respectively by papain (Pierce) digestion according to the manufacturer's instruction and subsequently purified by gel filtration on a Superdex 200 10/300 GL (GE Healthcare) in a buffer containing 20 mM Tris and 150 mM NaCl (pH 8.0). GY-14-single-chain variable fragment (scFv) was constructed as VL-$(GGGGS)_4$-VH which expressed and refolded as described previously (Liu et al., 2017; He et al., 2017; Tan et al., 2018). Recombinant GY-14-scFv were further purified by Superdex 200 10/300 GL

(GE Healthcare) chromatography.

The H chain and L chain of chimeric GY-5 and GY-14 constructed with human IgG4 subtype were cloned into pCAGGS plasmids with *EcoR*I and *Bgl*II restriction sites. The H chain and L chain plasmids of chimeric GY-5 and GY-14 were transiently co-transfected into HEK 293 T cells (ATCC) for protein expression. The protein was purified using a Protein G affinity column (GE Healthcare) and subsequently purified by gel filtration on a Superdex 200 10/300 GL (GE Healthcare) in a buffer containing 20 mM Tris (pH 8.0) and 150 mM NaCl.

Mouse model for anti-PD-1 antibody treatment.

Highly immunodeficient NCG mice (Model Animal Research Center of Nanjing University) were injected with human PBMC *i.v.* 3 days prior to engraftment of HCC-827 NSCLC cells. Then the mice were inoculated with NSCLC cells into one of the flanks of each mouse (5×10^6 cells/mouse) subcutaneously. Three days after engraftment, GY-5, GY-14 or 13C6 (anti-Ebola virus antibody) antibody was injected *i.p.* at 10 mg/kg twice a week. Growth rates were determined by measuring three dimensions (length, width and depth) of tumors with calipers twice a week. After 4 weeks, mice were sacrificed with a CO_2 chamber. Volumes of tumors were calculated according to the formula: Volume = length × width × height × 0.5236. Animal care was carried out in accordance with the guidelines of Animal Care and Use Committee of Institute of Microbiology, Chinese Academy of Sciences.

Flow cytometry of PD-1/PD-L1 blockade assay

The full-length PD-L1 was cloned into pEGFP-N1 vector (Clontech). HEK 293 T cells were transiently transfected with this recombinant plasmid for 24 hours and resuspended in PBS at 1×10^7 cells/mL. PD-1-mFc protein at a concentration of 2 μg/mL and GY-5 or GY-14 antibody at a concentration of 20 μg/mL were pre-incubated respectively at room temperature for 30 minutes. Then these mixtures were used to incubate with the 293T cells expressing PD-L1 fused EGFP protein at room temperature for further 30 min. After washing with PBS for three times, the cells were stained with secondary APC-anti-human IgG (Clone G18-145, BD Pharmingen) for another 30 min and analyzed using flow cytometry (BD FACSCalibur Flow Cytometer).

Enzyme-linked immunospot (ELISpot) assay

Peripheral blood mononuclear cells (PBMCs) from three healthy donors were isolated by use of the Ficoll-Paque gradient technique according to the manufacturer's instruction (Hao Yang Biological Manufacture). PBMCs isolated were incubated respectively with M1 peptide pool (Liu et al., 2016) (10 μg/mL) after culturing in the 24-well-plate for 24 hours . Recombinant interleukin 2 (IL-2) at a concentration of 50 UI/mL was added to the culture medium on day 3. The next day, half of the medium from the plate was replaced with fresh RPMI-1640 media (Gibco, Thermo Fisher Scientific). On day 7, the PBMCs were seeded on the ELISpot plate (BD) with M1 peptide pool (10 μg/mL) and PD-1 specific MAbs (10 μg/mL). PBMCs incubated with medium alone were enrolled as mock while PBMCs stimulated with M1 peptide pool

alone or together with Ebola virus GP protein specific 13C6 MAb were served as negative control. Secretion of IFN-γ from activated T cells was examined by the ELISpot assay kit (Human IFN-γ Set, BD) following the manufacturer's instructions. The reaction was finally stopped using demineralized water and spots were analyzed with an ELISpot reader (ImmunoSpot® S6 analyzers, Cellular Technology).

Surface plasmon resonance (SPR)

SPR measurements were done at room temperature using a BIAcore®T100 system with CM5 chips (GE Healthcare). For all measurements, the buffer consisting of 150 mM NaCl, 10 mM HEPES, pH 7.4 and 0.005% (v/v) Tween-20 was used as running buffer, and all proteins were exchanged into this buffer in advance through gel filtration. The blank channel of the chip served as the negative control. To detect the anti-PD-1 antibodies binding to PD-1 proteins, full-length GY-5 or GY-14 was immobilized on the chip at a concentration of 1 mg/mL by anti-human IgG at B70 response units. Gradient concentrations of PD-1 (0 nM, 3.125 nM, 6.25 nM, 12.5 nM, 25 nM and 50 nM) were then flowed over the chip surface. After each cycle, the sensor surface was regenerated with 3M $MgCl_2$. The binding kinetics were all analyzed with the software of BIA evaluation Version 4.1 using a 1:1 Langmuir-binding model.

Crystal screening and structure determination

PD-1 protein expressed in insect cells and GY-5-Fab, or PD-1 proteins refolded from inclusion bodies from *E. coli* cells and GY-14-scFv were mixed respectively at a molar

ratio of 1:1. The mixed samples were incubated for 30 min on ice and then purified by gel-filtration. Pooled proteins (10 mg/mL) were used for crystal screening by vapor-diffusion sitting-drop method at 4 ºC. Diffracting crystals of PD-1/GY-5 were obtained in conditions consisting of 0.1 M citrate (pH 5.0), 20% w/v polyethylene glycol 6,000 and 0.2 M ammonium acetate, while crystals of PD-1/GY-14 were obtained in conditions consisting of 0.06 M $MgCl_2$ and $CaCl_2$, 0.1 M imidazole-MES (pH 6.5), 18% v/v ethylene glycol and polyethylene glycol 8,000, respectively. After incubation in a reservoir solution containing 20% (v/v) glycerol crystals were flash-cooled in liquid nitrogen. The diffraction data were collected at Shanghai Synchrotron Radiation Facility BL17U, and all data were processed with HKL2000 (Otwinowski and Minor, 1997). The complex structure was solved by molecular replacement method using Phaser (Read et al., 2001) from the CCP4 programme suite (Collaborative computational project N, 1994), with the reported PD-1 structure (PDB: 3RRQ) and Fab structure (PDB: 3EYQ) as the search models. COOT (Emsley and Cowtan, 2004) and PHENIX (Adams et al., 2010) were used for subsequent model building and refinement. The stereochemical qualities of the final model were assessed with MolProbity (Chen et al., 2010). All structure figures were prepared with Pymol (http://www.pymol.org).

Data and software availability

The accession number for the atomic coordinates of GY-5/PD-1 complex and GY-14/PD-1 complex reported in this paper is PDB: 6J15 and 6J14.

Supplemental References

Adams, P. D., Afonine, P.V., Bunkóczi, G., Chen, V.B., Davis, I.W., Echols, N., Headd, J.J., Hung, L.W., Kapral, G.J., Grosse-Kunstleve, R.W., et al. (2010). PHENIX: a comprehensive Python-based system for macromolecular structure solution. Acta Crystallogr. D Biol. Crystallogr. *66*, 213-221.

Chen, V.B., Arendall, W.B.3rd., Headd, J.J., Keedy, D.A., Immormino, R.M., Kapral, G.J., Murray, L.W., Richardson, J.S., Richardson, D.C., et al. (2010). MolProbity: all-atom structure validation for macromolecular crystallography. Acta Crystallogr. D Biol. Crystallogr. *66*, 12-21.

Collaborative computational project N. (1994). The CCP4 suite: programs for protein crystallography. Acta Crystallogr. D Biol. Crystallogr. *50*, 760-763.

Emsley, P. and Cowtan, K. (2004). Coot: model-building tools for molecular graphics. Acta Crystallogr. D Biol. Crystallogr. *60*, 2126-2132.

He, M., Chai, Y., Qi, J., Zhang, C.W., Tong, Z., Shi, Y., Yan, J., Tan, S., Gao, G.F. (2017). Remarkably similar CTLA-4 binding properties of therapeutic ipilimumab and tremelimumab antibodies. Oncotarget *8*, 67129-67139.

Li, H., Zhou, M., Han, J., Zhu, X., Dong, T., Gao, G.F., Tien, P. (2005). Generation of murine CTL by a hepatitis B virus-specific peptide and evaluation of the adjuvant effect of heat shock protein glycoprotein 96 and its terminal fragments. J. Immunol. *174*, 195-204.

Liu, K., Tan, S., Chai, Y., Chen, D., Song, H., Zhang, C.W., Shi, Y., Liu, J., Tan, W., Lyu, J., et al. (2017). Structural basis of anti-PD-L1 monoclonal antibody avelumab for tumor therapy. Cell Res. *27*, 151-153.

Otwinowski, Z. and Minor, W. (1997). Processing of X-ray diffraction data collected in oscillation mode. Methods Enzymol. *276*, 307-326.

Read, R. J. (2001). Pushing the boundaries of molecular replacement with maximum likelihood. Acta Crystallogr. D Biol. Crystallogr. *57*, 1373-1382.

Tan, S., Zhang, H., Chai, Y., Song, H., Tong, Z., Wang, Q., Qi, J., Wong, G., Zhu, X., Liu, W.J., et al. (2017). An unexpected N-terminal loop in PD-1 dominates binding by nivolumab. Nat. Commun. *8*, 14369.

Tan, S., Liu, K., Chai, Y., Zhang, C.W., Gao, S., Gao, G.F., Qi, J., et al. (2018). Distinct PD-L1 binding characteristics of therapeutic monoclonal antibody durvalumab. Protein Cell *9*, 135-139.